

# Vibration Reduction Method by Instantaneous Current Control in 120-degree Conduction Mode of Compressor Motor

Yusuke Omi, Takumi Yasuda, Takahiro Kumagai, Hiroki Watanabe and Jun-ichi Itoh

NAGAOKA UNIVERSITY OF TECHNOLOGY

1603-1, Kamitomioka-machi, Nagaoka, Niigata, Japan

Tel.: +81 / (258) – 47.9533.

E-Mail: s203129@stn.nagaokaut.ac.jp, t\_yasuda@stn.nagaokaut.ac.jp,  
kumagai\_t1125@stn.nagaokaut.ac.jp, hwatanabe@vos.nagaokaut.ac.jp,  
itoh@vos.nagaokaut.ac.jp

URL: <http://itohserver01.nagaokaut.ac.jp/itohlab/jp/index.html>

## Keywords

«PMSM», «Compressor», «Three-phase motor drive», «Vibration suppression», «Sensorless control».

## Abstract

This paper proposes the vibration suppression method for compressors driven in 120-degree conduction mode. The load torque characteristic of the compressor fluctuates in one period of the mechanical angle. Thus, the speed ripple occurs in the motor, and the compressor vibrates. Therefore, this paper proposes a vibration reduction method with an instantaneous current control with a disturbance observer for the compressor driven by the 120-degree conduction mode. The feature of this paper is that motor speed is estimated by the back electromotive force (EMF) of the open phase due to the 120-degree conduction mode drive. The proposed method is verified experimentally under a limited loaded condition of the compressor as a fundamental study. As a result, the proposed control method reduces the fundamental frequency component of the vibration by 66.4% at a low speed of 0.19 p.u.

## Introduction

Home appliance applications, such as air conditioners and refrigerators, are required to be not only compact and highly efficient but also have low acoustic noise and low vibration. These home appliances use compressors in order to obtain a high-pressure refrigerant. The compressor repeats the cycle of (1) suction, (2) compression, and (3) discharge for heat exchange. This repetitive operation causes a load torque fluctuation and speed ripple in the motor. Besides,

the motor is sealed inside the compressor case. In addition, speed sensors and position sensors cannot be attached to the motor because the inside of the compressor case is high temperature and high pressure.

Interior Permanent Magnetic Synchronous Motors (IPMSMs) are often used for the compressor drive in home appliances thanks to their distinct advantages of high power density and high efficiency [1]-[4]. A vibration reduction method based on the position sensorless control for the IPMSM using the Fourier transform and repetitive control has been introduced [5]. The estimated load torque variation is compensated using a simplified Fourier transform and inverse transform [6]. However, these methods control the current in the rotating reference frame and require complex calculations for the sensorless vector control (Field orient control), including the coordinate transformations. Thus, a microcontroller with high processing power is required. Then it may increase product costs.

In order to solve these problems, this paper proposes a vibration reduction method with an instantaneous current control and feedforward current command for the compressor driven by the 120-degree conduction mode. In 120-degree conduction mode, the rotor position and motor speed are estimated by detecting the back EMF of the open phase [7]. Thus, complex calculations and motor parameters are not required in 120-degree conduction mode. The feature of this paper is the minimization of the speed ripple caused by the load torque fluctuation with feedforward current commands obtained by the disturbance observer. The proposed method is verified experimentally under a limited-loaded condition of the compressor as a fundamental study. The feedforward current command in the experiment was generated according to the

mechanical angle by a look-up table. The mechanical angle estimation is also proposed from the electric and offset angles in this paper.

First, this paper clarifies the cause of vibration when the compressor is driven in 120-degree conduction mode. Next, this paper shows that the proposed controller based on the disturbance observer suppresses the vibration when the motor speed is estimated completely in simulation. Finally, the proposed method demonstrates an experiment with a compressor. The experimental results show that the proposed control reduces the fundamental frequency component of the vibration by 66.4% at a low speed of 0.19 p.u.

## Drive system for compressor drive motors

### A. Characteristics of compressor

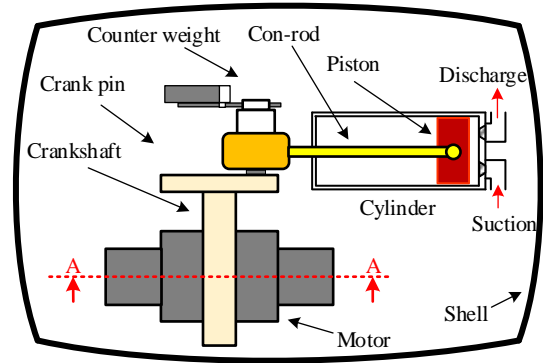
Fig. 1 shows a schematic diagram of a reciprocating compressor considered in this paper. The reciprocating compressor periodically switches three processes (1) the suction, (2) the compression, and (3) the ejection by the rotation of the rotor. Fig. 1(a) shows a piston at the top dead center, which is defined as a state that the piston is closest to the cylinder wall. Fig. 1(b) shows the piston at the bottom dead center, where the piston is farthest from the cylinder wall. In this paper, the mechanical angle  $\theta_{mech}$  at the top dead center is defined as 0 degrees.

Fig. 2 shows a cross-sectional view of the compressor drive motor at the top dead center (Fig. 1(a)). This paper uses a six-pole motor with three couples of the magnet. Fig. 2(b) is an enlarged view of the area around the magnetic pole  $N1$  in Fig. 2(a). The mechanical and electrical angle difference  $\theta_b$  is defined as a phase difference between the reference of the mechanical angle (TDC position) and the stator magnetic pole  $N1$ , as shown in Fig. 2(b).

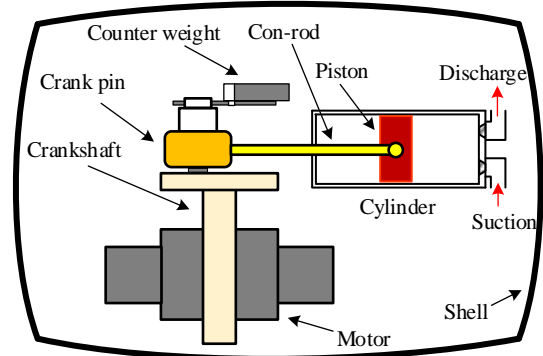
Fig. 3 shows the load torque characteristic of the compressor with respect to the mechanical and electrical angle difference  $\theta_b$  and the electrical angle. The load torque characteristic of the compressor fluctuates in one period of the mechanical angle. In addition, the load torque characteristic is determined by the discharge pressure  $P_d$  and suction pressure  $P_s$  of the refrigerant in the compressor [8]. 0 degree of the electrical angle at the stator magnetic pole  $N1$  becomes the mechanical angle of  $\theta_b$ .

### B. Sensorless 120-degree conduction drive

Fig. 4 shows a conceptual diagram of the 120-degree conduction mode. The voltage is applied



(a) Top dead center ( $\theta_{mech} = 0$  degrees).



(b) Bottom dead center ( $\theta_{mech} = 180$  degrees).

Fig. 1. Scheme drawings of compressor.

to the two phases corresponding to the estimated electrical angle, and the phases are switched every 60 degrees. The current is controlled by adjusting the output voltage by PWM. The electrical angle is estimated by detecting the zero-crossing point of the back EMF. The zero-crossing point of the back EMF is detected during the open interval of each phase. The motor speed is estimated from the time interval between the detected zero-crossing points of the back EMF.

Fig. 5 shows the relationship between the conduction mode and the definition of the current in the 120-degree conduction mode. In the 120-degree conduction mode, the control current  $i_{ad}$  is defined as the average of the currents of the two conduction phases.

### C. Control strategy of motor drive system

Fig. 6 shows a general control block diagram for the compressor drive motor using the 120-degree conduction mode. Fig. 7 shows the circuit diagram of the three-phase inverter. The control block diagram mainly comprises a current control (ACR) and speed control (ASR). The rotation speed calculation estimates the speed from the zero-crossing detection signals ( $ZD_U$ ,  $ZD_V$ , and  $ZD_W$ ) of the back EMF in each phase. The zero-crossing detection signals are obtained by the star connection resistance connected to the inverter

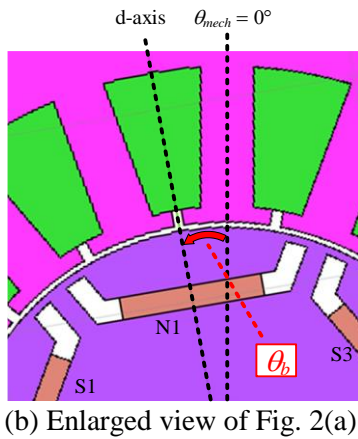
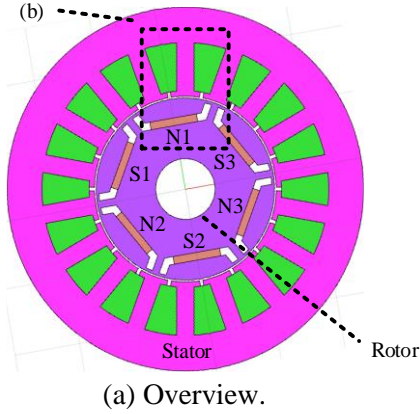
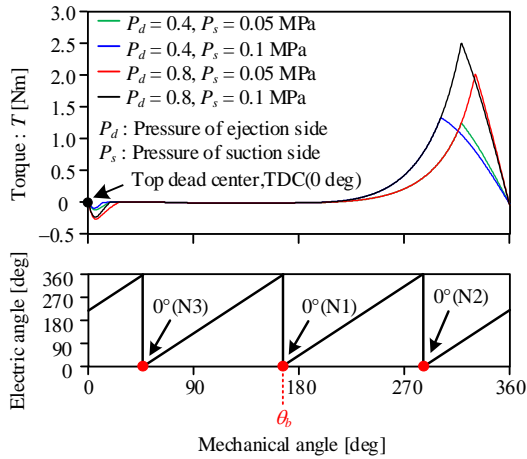


Fig. 2. Cross section of compressor motor at top dead center (Cross section of A-A in Fig. 1(a))



output, as shown in Fig. 7. The ASR regulates the average motor speed to the command value. Note that Fig. 6 omits the sequence from the startup to the transition to the sensorless control. The motor is first accelerated to the speed of 0.125 p.u. with the open-loop operation, which enables the

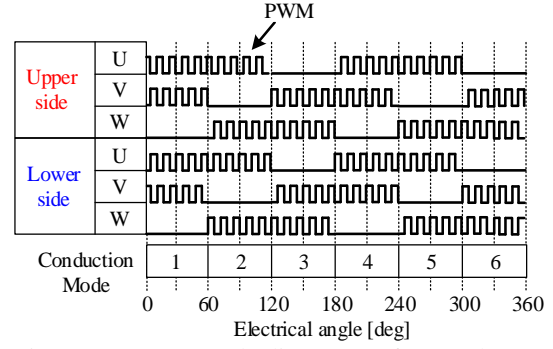


Fig. 4. Conceptual diagram of 120-degree conduction mode.

Conduction mode	1	2	3	4	5	6
Positive voltage application phase	U		V		W	
Negative voltage application phase	V		W		U	
Control current $i_{ad}$	$(I_u - I_v)$		$(I_u - I_w)$		$(I_v - I_w)$	
Electrical angle	0°	60°	120°	180°	240°	300°

Fig. 5. Relationship between conduction mode and control current.

detection of the back EMF [9]. Then, the control method is switched to the sensorless control.

## Analysis of compressor vibration factors

Fig. 8 shows the harmonic analysis of the compressor vibration at a speed command of 15 rps (0.19 p.u.). The compressor vibration is measured using the acceleration sensor (Ono Sokki, NP-3120) and the sensor amplifier (Ono Sokki, SR-2210, FLAT mode). The acceleration sensor is attached to the shell in the reciprocating direction of the piston in the compressor.

The harmonic analysis results indicate that the vibration occurs at the frequency component of the integral multiples of the mechanical angular frequency. On the other hand, the vibration of the integer multiples of the mechanical angular frequency is caused by periodic load torque fluctuations. In addition, the decrease in the amplitude of the with increasing harmonic orders is an effect of the mechanical frequency characteristics of the compressor. Besides, both vibration components around the switching frequency (16 kHz) and that at the 18th order frequency, generated by switching the conduction phase in the 120-degree conduction mode, are small. According to these results, the low-order frequency components of the load torque are the main cause of the vibration in the compressor

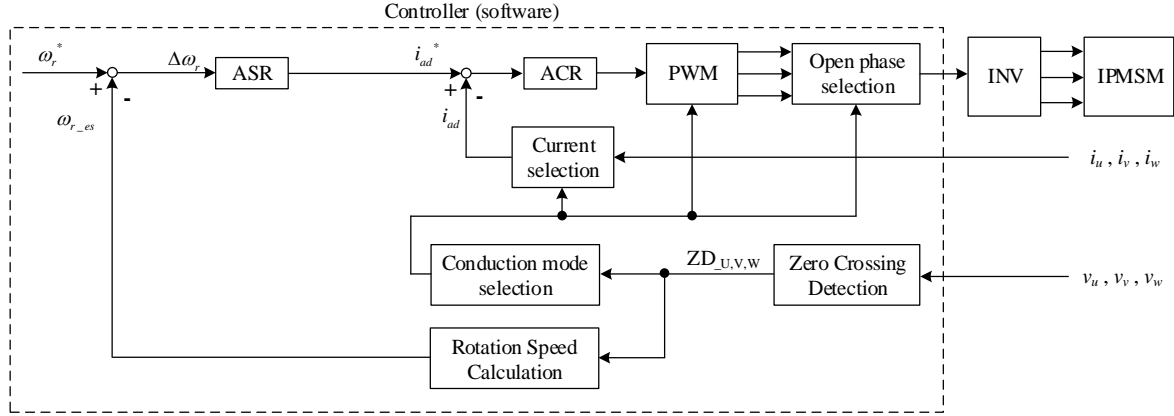


Fig. 6. Motor control configuration for compressor drive.

under the 120-degree conduction mode. Thus, it is necessary to suppress the vibration caused by the load torque.

## Proposed vibration suppression control

This paper proposes a vibration reduction method with an instantaneous current control and feedforward current command obtained by a disturbance observer for the compressor driven by the 120-degree conduction mode. First, this chapter explains the outline of the disturbance observer in the 120-degree conduction mode. Finally, the generation method of the compensation current command  $i_{DOB}$  with the disturbance observer is explained.

Fig. 9 shows the control block diagram of the disturbance observer. The disturbance observer is adopted to compensate for the load torque and suppress the vibration with  $i_{DOB}$ . The following subsection elaborates on the detail of the disturbance observer.

In Fig. 9,  $\Delta T$  is the difference between motor torque  $T_M$  and load torque  $T_L$ . Also,  $i_{dis}$  is the sum of the current that generates  $T_M$  and the current that generates  $-T_L$ . As shown in Fig. 9,  $\Delta T$  is obtained by differentiating the motor speed and multiplying the inertia, which is the inverse model of the internal model of the motor. Here, the relationship between  $i_{ad}$  and  $T_M$  is expressed as

$$T_M = \frac{3}{2}P \left\{ \psi_m i_{ad} \sin \theta + \frac{1}{2} (L_d - L_q) i_{ad}^2 \sin 2\theta \right\} \quad (1)$$

where  $P$  is the number of pole pairs,  $L_d$  is the d-axis inductance,  $L_q$  is the q-axis inductance,  $\psi_m$  is the field flux linkage, and  $\theta$  is the load angle. Inverse function of (1) is included in the disturbance observer to estimate  $i_{dis}$ . In the 120-

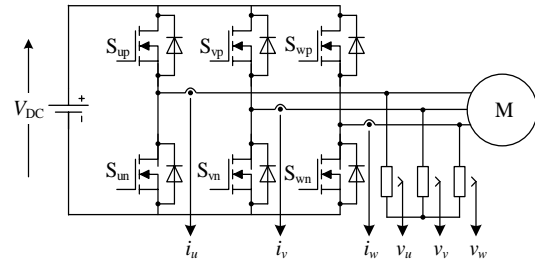


Fig.7. Circuit Configuration of Three-Phase Inverter.

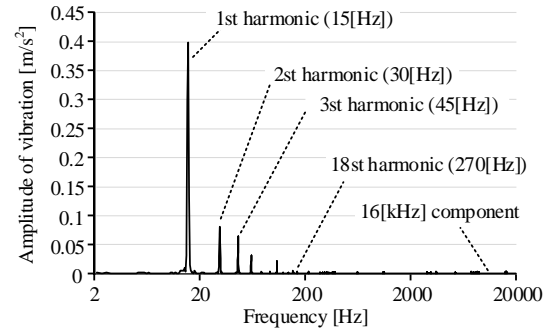


Fig. 8. Harmonic analysis results of vibration.

degree conduction mode, the load angle  $\theta$  continuously changes, unlike the vector control with  $i_d=0$  control. In this paper, the inverse function of (1) in the disturbance observer is simplified as (2), assuming the load angle  $\theta = 90^\circ$ .

$$i_{dis} = \frac{2\Delta T}{3P\psi_m} \quad (2)$$

The compensation current command  $i_{DOB}$  is derived by calculating the difference between  $i_{dis}$  calculated from (2) and the current command  $i_{ad\_LPF}^{**}$ , which is a low-pass filter applied to the compressor current command  $i_{ad}^{**}$ .

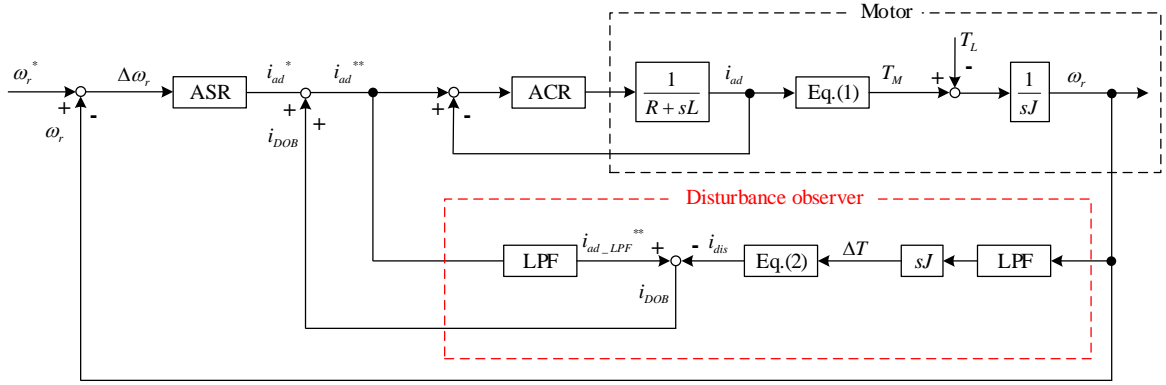


Fig. 9. Control block diagram of disturbance observer

## Validation by simulation

This chapter shows that the proposed controller with the disturbance observer reduces the motor speed ripple when the motor speed is estimated completely in simulation. Finally, the effect of reducing the motor speed ripple is confirmed in the simulation.

### A. Simulation conditions

As shown in Fig. 9, the disturbance observer feeds back the actual speed instead of the speed estimated from the back EMF. This reason is explained below.

Table 1 shows the motor parameters and the simulation conditions. The motor speed ripple is evaluated at a low speed of 0.19p.u. When the motor is actually driven in 120-degree conduction mode, sampling of the estimated speed detection is slow. Therefore, the response frequency of the ASR is set low. In addition, the response frequency of the ACR is large in order to improve the follow-up to the compensation current. Furthermore, the cutoff frequency of the low-pass filter is set to 20 times the mechanical angular frequency.

### B. Simulation results

Fig. 10 shows simulation results of the motor speed, the compressor current command  $i_{ad}^{**}$ , and load torque waveforms with and without the disturbance observer. Fig. 10(a) shows the simulation results when  $i_{DOB}$  is set to zero, and Fig. 10(b) shows the results when the load torque is compensated by the disturbance observer. As shown in Fig. 10(a), the current command is almost constant regardless of the change in the load torque. Therefore, the motor speed decreases significantly as the load torque increases, which results in a large speed ripple. On the other hand, as shown in Fig. 10(b), the current command changes according to the load torque due to the

Table. 1. Simulation conditions.

Parameter	Symbol	Value
Rating rotation speed	$\omega_n$	80 rps
Rating torque	$T_n$	0.237 N·m
Number of pole pairs	$P$	3
Winding resistance	$R$	6.2 $\Omega$
d-axis inductance	$L_d$	76.3 mH
q-axis inductance	$L_q$	136 mH
Field flux linkage	$\Psi_m$	0.14 Wb
Inertia moment	$J$	0.00037 kgm <sup>2</sup>
DC-link voltage	$V_{dc}$	280 V
Switching frequency	$f_{sw}$	16 kHz
Speed command value	$\omega_r^*$	15 rps

disturbance observer. As a result, the motor speed ripple is suppressed.

Fig. 11 shows the harmonic analysis results of the motor speed without and with the disturbance observer. The harmonic analysis results show that the fundamental frequency component of the motor speed is reduced by 95.4% thanks to the disturbance observer. Furthermore, the frequency component at integer multiples of the fundamental frequency is also reduced.

These results indicate that the speed ripple caused by the load torque is reduced by applying the disturbance observer.

In the 120° conduction mode, the motor speed is estimated from the interval between zero-crossing signals of the back EMFs. Therefore, the detection performances, such as resolution, response, and accuracy, depend on the motor speed in the 120° conduction mode. Especially the detection performance will be decreased in low speed regions. Besides, a large speed error occurs in the estimated speed due to including the load torque fluctuation of high frequency. Therefore, a disturbance is expected to be difficult to estimate accurately when the disturbance observer is applied using the estimated speed. Thus, vibration suppression by the disturbance observer is difficult in the 120-degree conduction mode at this time.

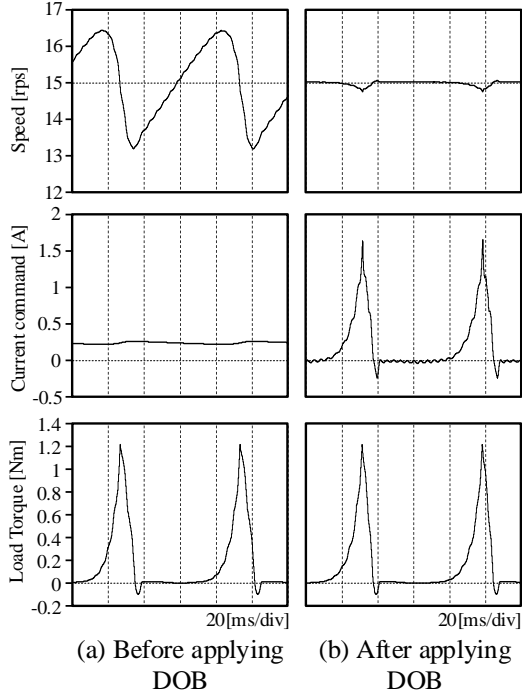


Fig.10. Waveform of the motor speed, compressor current command  $i_{ad}^{**}$ , and load torque with and without the disturbance observer.

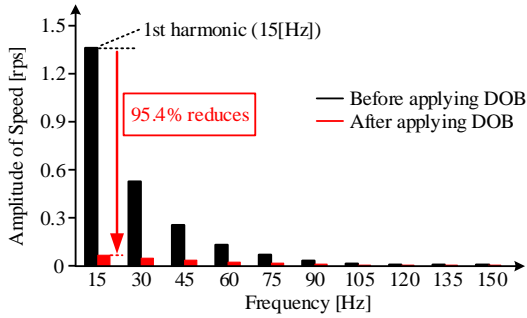


Fig. 11. Harmonic analysis results of Motor speed.

## Validation by experiment

The previous chapter showed that the disturbance observer reduces the motor speed ripple when the motor speed is completely estimated in simulation. However, a disturbance was expected to be difficult to estimate accurately at low speed.

Therefore, as a fundamental study to confirm the effectiveness of the feedforward current command control, this paper uses feedforward compensation current commands under constant load torque characteristic conditions through experiments. Here, the feedforward compensation current command  $i_{comp}$  is derived

from the known load torque characteristics. In addition, the value of  $i_{comp}$  changes according to the mechanical angle. In this chapter, first, the outline of the proposed control method is explained. Next, the mechanical angle estimation method is explained. Finally, the results of the experiment are shown by driving the compressor.

### A. Overview of the disturbance compensator

Fig. 12 shows the control block diagram of the disturbance compensator. The proposed control adds the feedforward compensation current command  $i_{comp}$  to the current command  $i_{ad}^*$  from the ASR to obtain the compressor motor current command  $i_{ad}^{**}$ . Furthermore, speed control and vibration suppression are achieved by controlling the current based on  $i_{ad}^{**}$ .  $i_{comp}$  is calculated by Equation (2) using the known load torque characteristics. Fig. 13 shows  $i_{comp}$  calculated by equation (2). As shown in Fig. 13,  $i_{comp}$  changes with the mechanical angle. This is because the load torque of the compressor changes with the mechanical angle. In this paper,  $i_{comp}$  is memorized in the look-up table and output according to the estimated mechanical angle  $\theta_{mech\_es}$ .  $\theta_{mech\_es}$  is calculated from the electrical angle obtained in 120-degree conduction mode and the offset angle  $\theta_b$ . The next subsection explains the method for estimating the machine angle.

### B. Mechanical Angle Estimation

The mechanical angle estimation is required to suppress the speed ripple with  $i_{comp}$  obtained in the last subsection.

Fig. 14 shows the relationship between the motor speed and the electric angle based on each pole, assuming that the motor is driven only with speed control (ASR). The motor torque is almost constant because the response frequency of the ASR is low. Then, the current command from the ASR can be treated as a constant over the mechanical period. On the other hand, the load torque fluctuates with the mechanical period, as shown in Fig. 3. As a result, the motor speed has ripples with the fundamental mechanical frequency. As shown in Fig. 14, the average speed of the motor over one electrical angle differs depending on the magnetic poles. As shown in Fig. 14, the electrical angle based on the magnetic pole N1 is the shortest in three electrical periods. The proposed method estimates the magnetic pole by comparing the average speed in the electrical period based on each magnetic pole. The mechanical angle estimation block in Fig. 12 outputs the mechanical angle synchronized to the electrical angle based on the magnetic pole N1 as

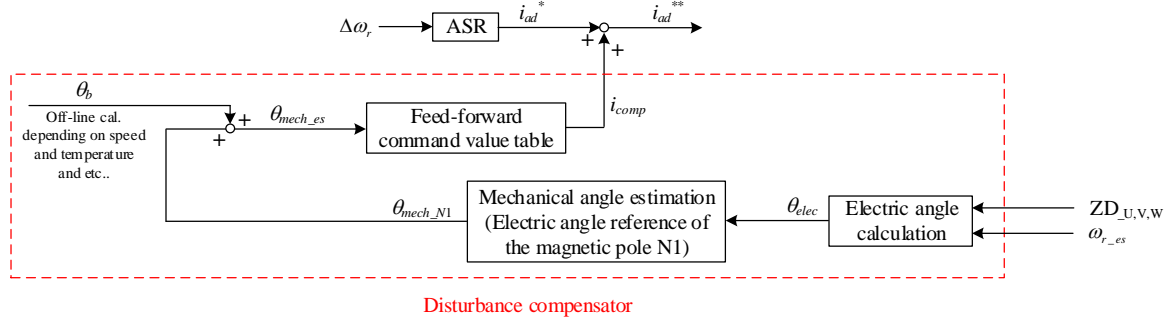


Fig. 12. Control block diagram of disturbance compensator

$\theta_{mech\_N1}$ . Note that  $\theta_{mech\_N1}$  has a phase error from the mechanical angle defined in Fig. 3. This is because the mechanical angle is an angle that depends on the arrangement of the crankshaft and piston. Thus,  $\theta_b$  is added to adjust the offset in  $\theta_{mech\_N1}$  and obtain  $\theta_{mech\_es}$ . In this paper,  $\theta_b$  is obtained from the back EMF when the compressor motor is free-running.  $\theta_b$  is estimated using the motor speed, load torque, and electric angle obtained from the back EMF. As a result of the free-run test,  $\theta_b$  was determined at 170 degrees.

### C. Experimental results

The motor parameters and experimental conditions are the same as the simulation conditions in Table 1. The compressor vibration is evaluated at a low speed of 0.19p.u.

Fig. 15 shows the calculation process of the modified estimated mechanical angle  $\theta_{mech\_m}$ . As shown in Fig. 15,  $\theta_{mech\_N1}$  is synchronized to the electric angle based on the magnetic pole N1 by the proposed method. Furthermore,  $\theta_b$  (= 170 degrees) is added to  $\theta_{mech\_N1}$  to obtain the estimated mechanical angle  $\theta_{mech\_es}$ , as shown in the bottom waveform of Fig. 15. These results verify that the proposed method can estimate the mechanical angle from the electrical angle.

Fig. 16 shows the three-phase current waveforms with and without the proposed method. The amplitude of the three-phase current is almost constant when only the speed control by the ASR is applied, as shown in Fig. 16(a). On the other hand, in Fig. 16(b), the instantaneous current control with the FF current command changes the current amplitude in one period of the mechanical angle.

Fig. 17 compares the acceleration sensor output waveforms with and without applying the proposed method. In Fig. 17(a), the fundamental frequency component (15 Hz) of the vibration is large because the proposed method is not applied. However, in Fig. 17(b), the fundamental

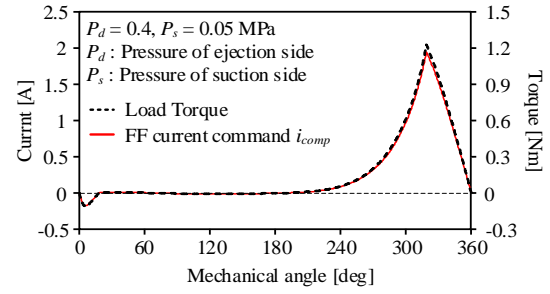


Fig. 13. Derived feedforward current command  $i_{comp}$

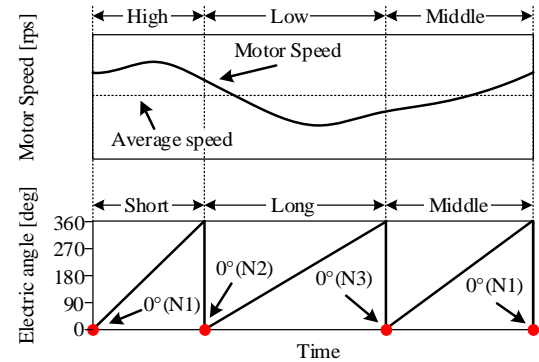


Fig. 14. Relationship between speed ripple and electric angle.

frequency component of the vibration is suppressed thanks to the proposed method.

Fig. 18 shows the harmonic analysis results of the vibration. The fundamental frequency component of the vibration is dominant when the proposed method is disabled. The proposed method suppressed the fundamental frequency component of the vibration by 66.4%. In addition, the vibration components of integer multiples of the fundamental frequency were also reduced.

## Conclusion

This paper proposed a vibration reduction method with an instantaneous current control and disturbance observer for the compressor driven by the 120-degree conduction mode. The proposed method is verified experimentally under

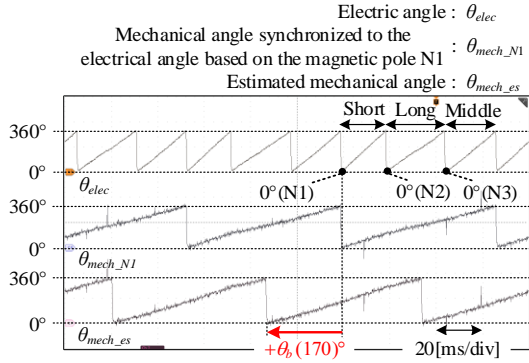
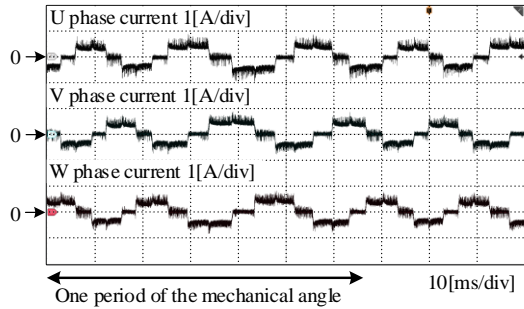
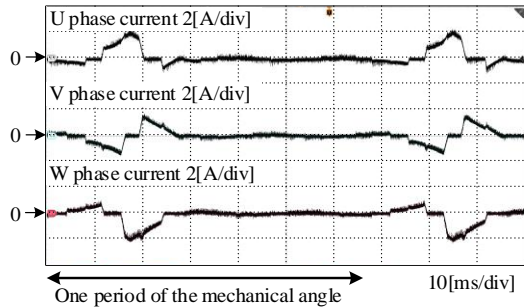


Fig. 15. Derivation process of  $\theta_{mech\_es}$



(a) Speed control by ASR.

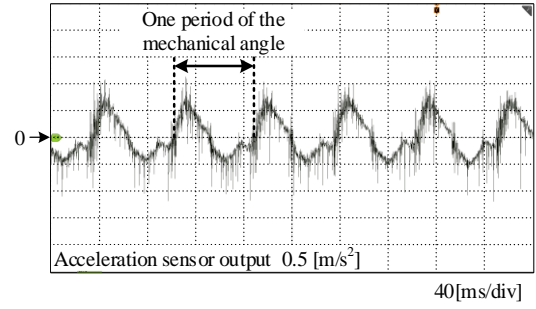


(b) Proposed method.

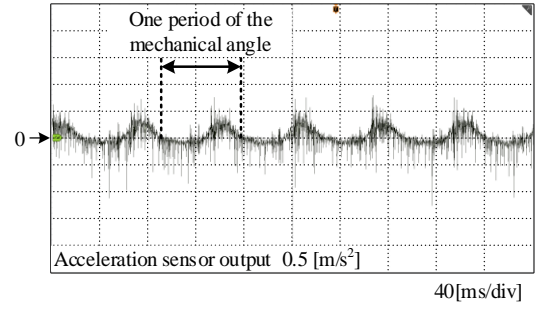
Fig. 16. Three-phase current waveforms.

a limited-load condition of the compressor as the fundamental study. In the fundamental study, the reference value that suppresses vibration is applied in feedforward according to the estimated mechanical angle. Thus, this method compensates for the load torque pulsation. As a result, the proposed control method reduces the fundamental frequency component of the vibration by 66.4% at a low speed of 0.19p.u.

In this paper, the compressor vibration was suppressed under constant speed and load torque characteristics. However, the load torque of a compressor changes with pressure conditions and motor speed. In future work, the validity of the disturbance observer will be verified through experiments.



(a) Speed control by ASR.



(b) Proposed method.

Fig. 17. Acceleration sensor output waveforms.

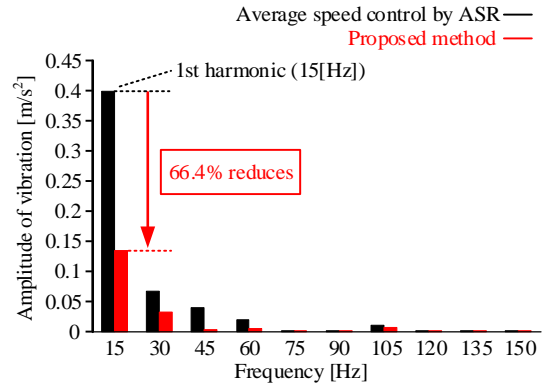


Fig. 18. Harmonic analysis results of vibration.

## References

- [1]. B. Hu; Z. Huang: "Linear Quadratic Extended State Observer based Load Torque Compensation for PMSM in a Single Rotor Compressor", 2019 22nd International Conference on Electrical Machines and Systems (ICEMS), Harbin, China, 2019
- [2]. K. Lee, S. Park and S. Jeong, "A Seamless Transition Control of Sensorless PMSM Compressor Drives for Improving Efficiency Based on a Dual-Mode Operation," in IEEE Transactions on Power Electronics, vol. 30, no. 3, pp. 1446-1456, March 2015
- [3]. K. Lee, J. Hong, S. B. Lee and S. Lee, "Quality Assurance Testing for Magnetization Quality Assessment of BLDC Motors Used in

Compressors," in IEEE Transactions on Industry Applications, vol. 46, no. 6, pp. 2452-2458, Nov.-Dec. 2010

[4]. Toshihiko Noguchi, "Trends of permanent-magnet synchronous machine drives," IEEJ Transaction on electrical and electronic engineering, Vol.2, No.2, pp.125-142, Feb. 2007

[5]. S. Hattori, "Vibration Suppression Control Method for PMSMs Based on Learning Control Corresponding to Operating Point Changes," in IEEJ Transactions on Industry Applications, vol. 137, no. 1, pp. 10-16, Jan. 2017 (in Japanese)

[6]. Y. Notohara, D. Li, Y. Iwaji, M. Tamura, and K. Tsukii, "Study on Vibration Suppression Control for Rotary Compressor," in IEEJ Transactions on Industry Applications, vol. 140, no. 11, pp. 841-847, Nov. 2020 (in Japanese)

[7]. P. Damodharan and K. Vasudevan, "Sensorless Brushless DC Motor Drive Based on the Zero-Crossing Detection of Back Electromotive Force (EMF) From the Line Voltage Difference," in IEEE Transactions on Energy Conversion, vol. 25, no. 3, pp. 661-668, Sept. 2010

[8]. T. Shioi, T. Kumagai, K. Kusaka, and J. Itoh, "Estimation Method of Load Torque Characteristics and Mechanical Parameter for Reciprocating Compressor Considering Pressure variation," in IEE-Japan Industry Applications Society Conference, no. 4-4, pp. IV-95, August. 2021 (in Japanese)

[9]. J. Liu, T. A. Nondahl, J. Dai, S. Royak, and P. B. Schmidt, "Seamless Transition Scheme of Position Sensorless Control in Industrial Permanent Magnet Motor Drives With Output Filter and Transformer for Oil Pump Applications," in IEEE Transactions on Industry Applications, vol. 56, no. 3, pp. 2180-2189, May/June 2020